

Quantum State Designs from Minimally Random Quantum Circuits

Jonathon Riddell,¹ Katja Klobas,¹ and Bruno Bertini¹

¹*School of Physics and Astronomy, University of Birmingham, Edgbaston, Birmingham, B15 2TT, UK*
(Dated: March 10, 2025)

Random many-body states are both a useful tool to model certain physical systems and an important asset for quantum computation. Realising them, however, generally requires an exponential (in system size) amount of resources. Recent research has presented a way out by showing that one can generate random states, or more precisely a controlled approximation of them, by applying a quantum circuit built in terms of few-body unitary gates. Most of this research, however, has been focussed on the case of quantum circuits composed by completely random unitary gates. Here we consider what happens for circuits that, instead, involve a minimal degree of randomness. Specifically, we concentrate on two different settings: (a) brickwork quantum circuits with a single one-qudit random matrix at a boundary; (b) brickwork quantum circuits with fixed interactions but random one-qudit gates everywhere. We show that, for any given initial state, (a) and (b) produce a distribution of states approaching the Haar distribution in the limit of large circuit depth. More precisely, we show that the moments of the distribution produced by our circuits can approximate the ones of the Haar distribution in a depth proportional to the system size. Interestingly we find that in both Cases (a) and (b) the relaxation to the Haar distribution occurs in two steps — this is in contrast with what happens in fully random circuits. Moreover, we show that choosing appropriately the fixed interactions, for example taking the local gate to be a dual-unitary gate with high enough entangling power, minimally random circuits produce a Haar random distribution more rapidly than fully random circuits. In particular, dual-unitary circuits with maximal entangling power — i.e. perfect tensors — appear to provide the optimal quantum state design preparation for any design number.

I. INTRODUCTION

Recent years have seen increasing interest devoted to the realisation of many-body random states in extended quantum systems. In essence, this is because these objects provide useful models for the state of real physical systems in certain conditions — most notably black holes [1, 2] — and represent useful resources for quantum computation and for the concrete realisation of quantum technologies, e.g., they can be used for efficient implementations of quantum state tomography [3] and benchmarking [4].

The basic problem that the researchers had to solve is that realising many-body random states, or, equivalently, many-body random unitary matrices, is *hard*, i.e., requires an amount of resources scaling *exponentially* with the number of microscopic constituents [5]. The proposed solutions made use of the concept of *pseudorandomness* [6], i.e., instead of attempting to construct a bona fide random state one can try to reproduce a state that ‘looks’ random to all experiments that query it only a finite number of times k — a state with this property is referred to as a quantum state k -design [7].

Crucially, contrary to true random states, k -designs admit efficient realisations in terms of local quantum circuits [8–19], i.e., they can be systematically approximated by repeatedly applying unitary operations that only couple a small number of qudits at a time. Specifically, a seminal result has been to show that one can realise k -designs using local circuits whose depth is only linear in the number of qudits of the system [10, 11]. In fact, very recent breakthroughs have shown that one

can achieve poly-logarithmic scaling of the depth with the number of constituent qudits by gluing together logarithmic-size circuits [16, 18].

Nearly all of this research, however, has been focussed on the case where the quantum circuits realising the approximate k -designs are fully random (or are fully random modulo certain symmetries [15, 19]). A natural question is then whether the ‘approximate k -design property’ can be maintained when the amount of randomness is *reduced to a minimum*. For instance, when the random operations are restricted on a single qudit, while the rest of the circuit only involves *fixed* (non-random) operations.

This question is particularly compelling for two main reasons. First, by optimising the fixed operations one can hope to generate k -designs *more efficiently* than in fully random settings. In fact, the potential advantage is two-fold. On the one hand one would need to generate far less instances of the random circuit — the exponential scaling of the number of samples with the system size is avoided. On the other, by selecting an optimal circuit, one can hope to generate k -designs *faster* than the random circuit, i.e., requiring lower depth. Second, in the minimally random setting the emergence of (approximate) k -designs can be seen as a fascinating novel form of *universality* of the time evolution. Indeed, in the putative family of minimally random circuits producing approximate k -designs the dynamics becomes eventually insensitive to all the microscopic details (of both interactions and initial state). This would not only be the case for local observables as in regular thermalising systems [20, 21] but also for their multilinear functions up to

order k , hence displaying a form of thermalisation that is much stronger than the typical one — a similar stronger form of thermalisation has been recently observed in the context of *projected ensembles* [22–28].

Here we initiate the investigation of the aforementioned question. We first focus on the setting where a one-qudit random matrix is applied at the boundary of a one-dimensional brickwork circuit using a combination of numerical and analytical approaches. We consider two different classes of random one-qudit matrices: random Paulis — drawn with equal probability — and random unitary matrices — drawn from the Haar distribution. First, by adapting a theorem from Ref. [26], we show that for almost all choices of local gates of the quantum circuit this setting produces k -designs for sufficiently large times (i.e. circuit depths). Then we move on to characterise the time-scale of this process showing that, similarly to the fully random case [11–13], one can produce approximate k -designs in a number of time steps proportional to the number of qudits in the system. In fact, we find that if the local gates are close to being dual-unitary (DU) [29] and have sufficiently high entangling power the time scale to produce k -designs is strictly shorter than the Haar random circuit. Finally, we observe that, contrary to what happens for Haar random circuits, the generation of k -designs generically occurs in *two steps*.

We then move on to investigate a ‘more random’ setting that is still ‘less random’ than the Haar circuit. Our point of departure is that the two-step relaxation we identified has recently been found in the dynamics of purity [30–32] and out-of-time-ordered correlators [33, 34] in finite circuits of both fixed [34] and random gates [30–33]. The random circuits showing two-step relaxation, however, only involve *one-site* random operations while the two-qudit operation (the interaction) is fixed — some aspects of k -design generation in such systems have recently been studied in Ref. [35], which dubbed them *structured* random circuits. This behaviour was explained in Ref. [36] (see also Ref. [37]) by noting that both fixed and structured random gates can produce ‘magnon-like’ excitations in the multi-replica space that are not present in a fully random circuit. This suggests that structured random circuits should behave more similarly to fixed systems also concerning the generation of k -designs. We verify this hypothesis finding that all the behaviours observed in our minimally random circuits are also detected in structured random circuits. In fact, we find that random DU circuits with maximal entangling power show the fastest generation of k -designs.

The rest of the paper is laid out as follows. In Sec. II we describe in detail both settings considered in this paper — minimally random circuits and structured random circuits — and the main quantity of interest: the Frobenius distance between the k -moment density matrix of the brickwork circuit and the global Haar random one. In Sec. III we present a numerical survey of the evolution of this distance considering different choices of k and gate parameters. In Sec. IV we present an analytical charac-

terisation of these behaviours with special focus on the DU case, where more precise statements can be made. Finally, Sec. V contains our conclusions.

II. MINIMALLY RANDOM QUANTUM CIRCUITS

As discussed in the introduction, we are interested in the class of states generated by minimally random quantum circuits. In particular, we consider unitary circuits acting on $2L$ qudits ($d \geq 2$ internal states) with open boundary conditions and a brickwork structure of the form

$$\mathcal{U} = \mathcal{U}_e \mathcal{U}_o, \quad \mathcal{U}_e = \prod_{n=1}^L U_{2n,2n+1}^{(2n)}, \quad \mathcal{U}_o = \prod_{n=1}^{L-1} U_{2n+1,2n+2}^{(2n+1)}, \quad (1)$$

such that the time evolution of a state is written as

$$|\psi(t)\rangle = \mathcal{U}^t |\psi\rangle. \quad (2)$$

In Eq. (1) the operator $U_{a,b}^{(n)}$ acts non-trivially, as the matrix $U^{(n)} \in U(d)$, only on the qudits at position a and b and we have labeled the local gates with an additional superscript index to stress that these need-not be the same. We consider inserting randomness in two different ways

- (a) Random one-qudit unitaries on one of the boundaries (independent in time) and *fixed* gates everywhere else.
- (b) Random (and independent in the space-time) one-site gates everywhere but *fixed* two-site interactions.

In Case (a) one can express Eq. (1) at a given time step t as

$$\mathcal{U}(\alpha_t) = \mathcal{U}_e \mathcal{U}_o \cdot (\alpha_t)_{2L}, \quad (3)$$

where $\alpha_t \in S$ is a random one-site unitary matrix in the set S independently drawn with probability $\mu_S(\alpha_t)$ [38]. Case (b), instead, involves adding random one-site unitaries to every gate

$$U_{n,n+1}^{(n)} = (\alpha_t^{(n)} \otimes \alpha_t^{(n+1)}) \bar{U}_{n,n+1}^{(n)}, \quad (4)$$

where $\alpha_t^{(n)}$ and $\alpha_t^{(n+1)}$ are independently drawn from S and $\bar{U}_{n,n+1}^{(n)}$ is a fixed two-site unitary. Therefore, the time evolution operator at a given t depends on

$$\vec{\alpha}_t = (\alpha_{2t-1}^{(1)}, \dots, \alpha_{2t-1}^{(2L)}, \alpha_{2t}^{(1)}, \dots, \alpha_{2t}^{(2L)}) \quad (5)$$

random unitary matrices.

To treat both Cases (a) and (b) simultaneously we write $\mathcal{U}(\vec{\alpha}_t)$ where $\vec{\alpha}_t$ can either be a one-dimensional

or $4L$ -dimensional vector of unitary random matrices. Case (b) involves considerably more randomness compared to (a) but all of the entangling power of the circuit is contained in fixed, non-random two-local gates. We will see that this leads it to be closer to Case (a) than to a circuit with fully random interactions, like those studied in Refs. [8–18].

Given an initial state $|\psi\rangle$ we label its path through the random circuit with $\alpha_t = \{\vec{\alpha}_1, \vec{\alpha}_2, \dots, \vec{\alpha}_t\}$, i.e., we write the state at time t as $|\psi(\alpha_t)\rangle$. Therefore we denote the ensemble produced by our random circuits by

$$\mathcal{E} = \{\mu_S(\alpha_t), |\psi(\alpha_t)\rangle\}, \quad (6)$$

where $\mu_S(\alpha_t)$ is the probability of producing the state $|\psi(\alpha_t)\rangle$. Our independence condition implies that $\mu_S(\alpha_t)$ is the product of the probability measures for the individual $\alpha_t^{(n)}$. To fix the ideas here we consider three specific choices of d (local dimension), S , and μ_S

- (a.1) $d = 2$; $S = \{I, \sigma^x, \sigma^y, \sigma^z\}$; $\mu_S(\alpha) = 1/4$
- (a.2) d generic; $S = U(d)$; $\mu_S(\alpha) = \mu_H(\alpha)$
- (b.1) d generic; $S = U(d)^{4L}$; $\mu_S(\vec{\alpha}) = \prod_{j=1}^{4L} \mu_H(\alpha_j)$

where $\mu_H(\alpha)$ is the Haar measure of $U(d)$. We stress that the first two choices pertain to Case (a) while the third to Case (b).

We note that, by exchanging the roles of space and time, the ensemble produced by (a.1) becomes very similar to the projected ensemble considered in Refs. [26, 39]. Indeed, the application of a random Pauli becomes a measurement in the Pauli basis. Our setting, however, can produce more general ensembles because — contrary to Refs. [26, 39] — our local gates are *not* forced to be DU. Instead, as we mentioned in the introduction, random state generation in the setting (b.1) has recently been studied in Ref. [35], which dubbed it *structured* random unitary circuit. The latter reference, however, mostly focussed on gates fulfilling a special ‘solvable condition’ in the two-replica space.

Our main question is whether the distribution in Eq. (6) approaches the Haar distribution in the limit of large t and, in case, how it does so. To this end we study the time evolution of the moments of the distribution, which are captured by the mixed state

$$\rho_t^{(k)} = \mathbb{E} \left[(|\psi(\alpha_t)\rangle\langle\psi(\alpha_t)|)^{\otimes k} \right], \quad (7)$$

where the average is taken over the measure μ , i.e.

$$\mathbb{E}[f(\alpha_t)] = \sum_{\alpha_t \in S} f(\alpha_t) \mu_S(\alpha_t). \quad (8)$$

To quantify the convergence we investigate the two-norm distance of $\rho_t^{(k)}$ to the Haar ensemble

$$\Delta_2^{(k)}(t) = \frac{\|\rho_t^{(k)} - \rho_H^{(k)}\|_2^2}{\|\rho_H^{(k)}\|_2^2}, \quad (9)$$

where $\rho_H^{(k)}$ is written as Eq. (7) with μ replaced by the Haar measure. Here we have chosen the two-norm as it facilitates the analytical treatment. For instance, it allows us to express the distance between the ensembles in terms of *frame potentials* [40, 41]

$$F^{(k)} = \sum_{\alpha_t, \beta_t} \mu_{\alpha_t} \mu_{\beta_t} |\langle \psi_{\alpha_t} | \psi_{\beta_t} \rangle|^{2k} = \text{tr}[\rho^{(k)2}], \quad (10)$$

as follows

$$\Delta_2^{(k)} = \frac{F^{(k)}}{F_H^{(k)}} - 1, \quad (11)$$

where the frame potential for the Haar ensemble is known to be [41]

$$F_H^{(k)} = \binom{d^{2L} + k - 1}{k}^{-1}. \quad (12)$$

The key objective of this paper is to identify whether $\Delta_2^{(k)}(t)$ approaches 0 at large times and, if so, how large should one take t to have that $\Delta_2^{(k)}(t)$ is certainly smaller than some arbitrary ϵ [10, 11].

III. NUMERICAL SURVEY

To get some intuition on the behaviour of $\Delta_2^{(k)}(t)$ for large times we begin with a *numerical survey* considering both Cases (a) and (b). We focus our attention on a class of circuits with $d = 2$ characterized by the following parametrization

$$U_{n,n+1}^{(n)} = e^{i[J_x \sigma^x \otimes \sigma^x + J_y \sigma^y \otimes \sigma^y + J \sigma^z \otimes \sigma^z]} u_n \otimes u_{n+1}, \quad (13)$$

where $J_x = J_y = \pi/4 - \delta$ is fixed, and the one-site unitaries are characterized by fixed Euler angles

$$u = \exp[i\theta_1 \sigma^z] \exp[i\theta_2 \sigma^x] \exp[i\theta_3 \sigma^z]. \quad (14)$$

Moreover — unless we explicitly state otherwise — we take our initial state to be the all zero state

$$|\psi\rangle = |0\rangle^{\otimes 2L}. \quad (15)$$

Throughout this section δ is varied, however, we pay special attention to the point $\delta = 0$ where the circuit is DU. In Case (a) we fix $J = 0.1$ and randomly generate one realisation of the random Euler angles for each u_j , but we keep this fixed performing no average. In Case (b) the one-site unitaries $\{u_n\}$ are taken to be Haar random while we compare different J s. We discuss separately the two cases.

A. Case (a)

Since we have a single random unitary matrix at the boundary of the system (at $x = 2L$), in Case (a) we can

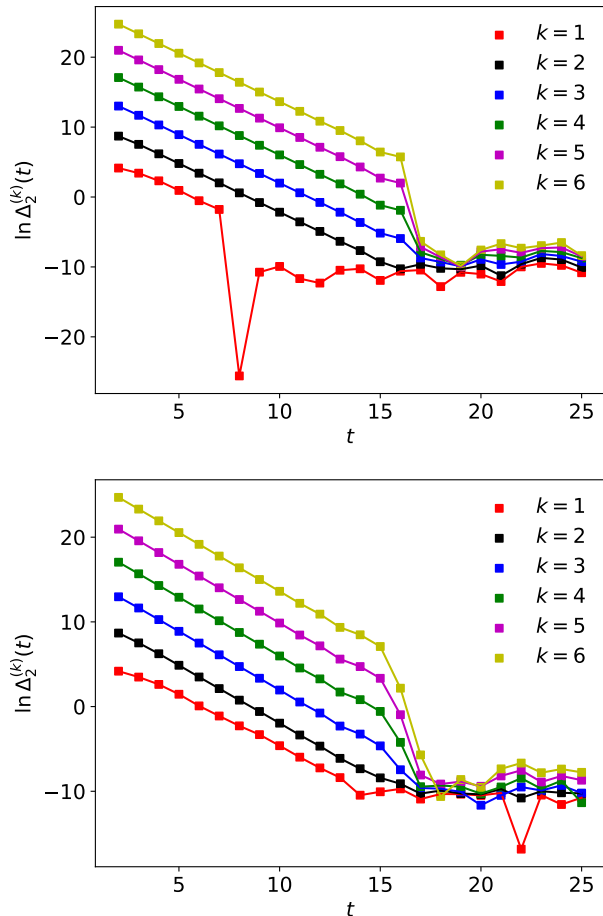


FIG. 1. Calculating $\Delta_2^{(k)}(t)$ with sampled averaging for $L = 4$ (8 qubits) for various k . Here we take random Pauli's on the boundary and evaluate the expression in Eq. (10) for all configurations for $t \leq 9$. For $t > 9$ we take 10^9 samples. We set $\delta = 0$ in the top figure and $\delta = 0.1$ in the bottom figure.

evaluate Eq. (9) in two ways: We can either compute the average explicitly and then calculate the dynamics, or numerically average over circuit realisations. Both approaches are discussed in more detail in Sec. IV.

First we perform the average numerically in the case of random Pauli matrices at the boundary, i.e., considering the choice (a.1) in the language of the previous section. We approximate the average by sampling a maximum of 10^9 configurations of Paulis. This allows us to access any moment k for $t \in [0, 9]$ exactly while larger t may be approximated: A representative example of our results is presented in the top panel of Fig. 1, which displays dynamics of the moments $k \in [1, 6]$ at the DU point ($\delta = 0$) and a non-DU point $\delta = 0.1$. We see that the distance seems to decay quickly in time, suggesting that the minimally random circuits do produce k -designs at large times — this statement can in fact be proved exactly as discussed in Sec. IV. Specifically, for $k > 1$ at the

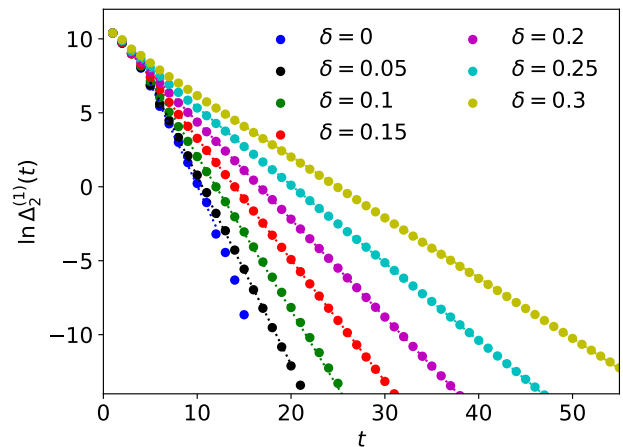


FIG. 2. Calculating $\Delta_2^{(1)}(t)$ with explicit averaging for $L = 8$ (16 qubits) for various δ . Curve captures the behaviour for both random Pauli and Haar averaging on the boundary.

DU point we see a common slope of

$$\ln \Delta_2^{(k)}(t) \approx -r_1^{(k)}t + c_1^{(k)}, \quad (16)$$

where $r_1^{(k)} \approx \ln 4 \approx 1.39$ at the DU point. For $k = 1$ the state $\rho_t^{(k)}$ reaches exactly the maximally mixed state — first moment of the Haar ensemble — in a finite number of steps equal to $2L + 1$. As we show in Sec. IV A, this is a direct consequence of dual-unitarity and it is well captured by the numerical average even at large times, when $4^{2t} \gg 10^9$. This can be partially explained by noting that the distribution of overlaps

$$\{|\langle \psi(\alpha_t) | \psi(\beta_t) \rangle|\}, \quad (17)$$

is *unimodal*. In fact, in App. B we show that the distribution of overlaps approaches a Rayleigh distribution [42] for large scales (time and system size) but is well approximated by it even at moderate scales. In the bottom figure of Fig. 1 we see the dynamics for a non-DU point with $\delta = 0.1$. Here the slope is again similar for all k but slower than the DU point with $r_1^{(k)} \approx 1.36$. Since we begin with a pure state for sufficiently large L we know $c_1^{(k)} \sim kL \ln 2$, which is found by applying the Stirling approximation to Eq. (12), regardless of δ or the initial pure state.

Sampling the configurations of α_t numerically becomes unfeasible for larger times. To progress, we evaluate the average in Eq. (7) explicitly, coupling together $2k$ copies of the system. In this way the evolution of $\rho_t^{(k)}$ is obtained by numerically constructing the superoperator $\mathcal{B}_k[\cdot]$ generating its dynamics (cf. Sec. IV), i.e.

$$\rho_{t+1}^{(k)} = \mathcal{B}_k[\rho_t^{(k)}]. \quad (18)$$

The operator \mathcal{B}_k inherits the brickwork structure from \mathbb{U} , but the local space of its gates is of dimension d^{2k} , rather

than d . This limits our investigation to $k = 1, 2$ but allows us to explore an essentially *arbitrary* time window.

The possibility of exploring large times reveals an interesting phenomenon. While away from the DU point $\Delta_2^{(k=1)}(t)$ shows a convincing exponential relaxation characterised by a single rate $r^{(1)}$, $\Delta_2^{(k=2)}(t)$ shows *two-step relaxation* of the form

$$\ln \Delta_2^{(2)}(t) \simeq \begin{cases} -r_1^{(2)}t + c_1^{(2)}, & t \leq t_*^{(2)} \\ -r_2^{(2)}t + c_2^{(2)} & t > t_*^{(2)} \end{cases}, \quad (19)$$

where $t_*^{(2)}$ is generically δ -dependent. A similar phenomenon was recently observed in the dynamics of purity [30–32] and out-of-time-ordered correlators [33, 34] in quantum circuits of finite size. First, in the case structured random circuits like those of our Case (b) [30–33], and then also in non-random cases [34]. This behaviour was explained in Ref. [36] (see also Ref. [37]) through a mapping to a statistical mechanical model (we comment more on this in Sec. IV A).

More specifically, our results for the case $k = 1$ are reported in Fig. 2. Note that these correspond to both choices (a.1) and (a.2) because for $k = 1$ the average over random Paulis and one-site random unitary matrices coincide. We already observed that in the DU case we have $\Delta_2^{(1)}(t \geq 2L) = 0$, while

$$r^{(1)} \Big|_{\substack{\delta=0 \\ t < 2L}} = \ln \frac{\Delta_2^{(1)}(t-1)}{\Delta_2^{(1)}(t)} \Big|_{\delta=0} = \ln d^2 = \ln 4. \quad (20)$$

Increasing δ , however, we observe a convincingly exponential decay after a few time steps for all $\delta > 0$. In particular, we have $r^{(1)}(\delta) \leq \ln 4$, meaning that even before relaxation the decay *is fastest at the DU point* and it is monotonically slower away from it. We demonstrate this in Fig. 3, where, for $\delta > 0$, $r_1^{(1)}$ shows a roughly exponential dependence on δ i.e.,

$$r_1^{(1)}(\delta) \approx \exp(-4.53\delta + c). \quad (21)$$

Next, we discuss our findings for $k = 2$, where the Cases (a.1) and (a.2) no longer result in the same dynamics. We see this in Fig. 4, which provides a comparison between the two (top and bottom panels). First we note that in this case the DU point does not show exact relaxation to the Haar value in a finite number of time-steps, however, it asymptotically flows to it faster than $\delta > 0$. We see a two step relaxation for both boundary drivings and all $\delta > 0$, while the DU point has an approximately flat decay with $r_1^{(2)} = r_2^{(2)} \sim \ln d^2 = \ln 4$ for Pauli driving and $r_1^{(2)} = r_2^{(2)} \sim \ln d^3 = \ln 8$ for Haar driving. In Fig. 5 we plot our extracted $r_1^{(2)}, r_2^{(2)}$ for both the cases studied. Close to the DU point the Haar driving is significantly faster than Pauli, while for sufficiently large δ the decay rates become equivalent. For both cases, all instances with $\delta < 0.15$ generate decay rates faster than that of

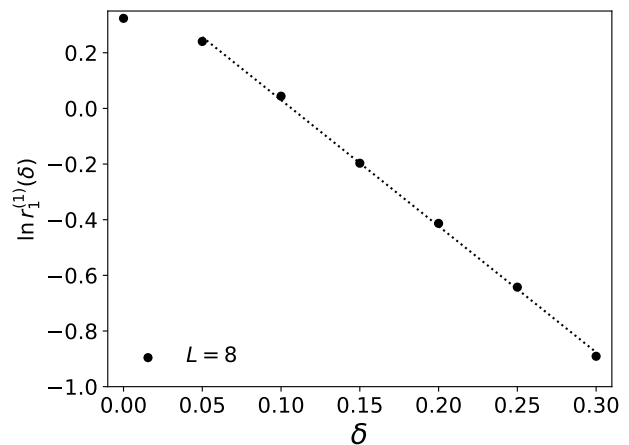


FIG. 3. $r_1^{(1)}$ for various δ extracted from the $L = 8$ (16 qubits) data presented in Fig. 2.

the Haar random brickwork circuit in the limit of large size (cf. [10–12, 35]), i.e.,

$$r_2^{(2)} \Big|_{\text{Haar}} = 4 \ln \frac{d^2 + 1}{2d}. \quad (22)$$

We also generically observe $r_1^{(2)} > r_2^{(2)}$.

Finally, Fig. 6 reports the transition time from the first to the second decay regime. We see weak dependence on δ when the latter is small, while the second decay regime takes over at later times for larger δ . The L dependence close to the DU point is consistent with $t_*^{(2)} = 2L$ for Haar driving and $t_*^{(2)} = 2L + 1$ for Pauli driving. Larger δ s appear to pick up a constant shift, so that for all δ s the scaling behaviour is consistent with $t_*^{(2)} \sim 2L$ for large L .

B. Case (b)

We now move to investigate an example of Case (b): Case (b.1) in the classification of Sec. II. Here we have Haar random unitary driving on every qudit for each time step but the two qudit interaction is fixed. The details on the specific implementation of this setting are presented in Sec. IV. For this class of circuits (and small k) we can study much larger systems due to the effective reduction in local dimension provided by the average over random one-site matrices everywhere. In light of the similar behaviours observed in the purity’s evolution (cf. Ref. [30–32]), we expect Case (b) to show similar phenomenology to Case (a).

In Fig. 7 we present results for the evolution of $\Delta_2^{(2)}(t)$ for different DU gates parametrised by their entangling power (cf. the discussion in Sec. IV B)

$$p = \frac{2}{3} \cos(2J)^2. \quad (23)$$

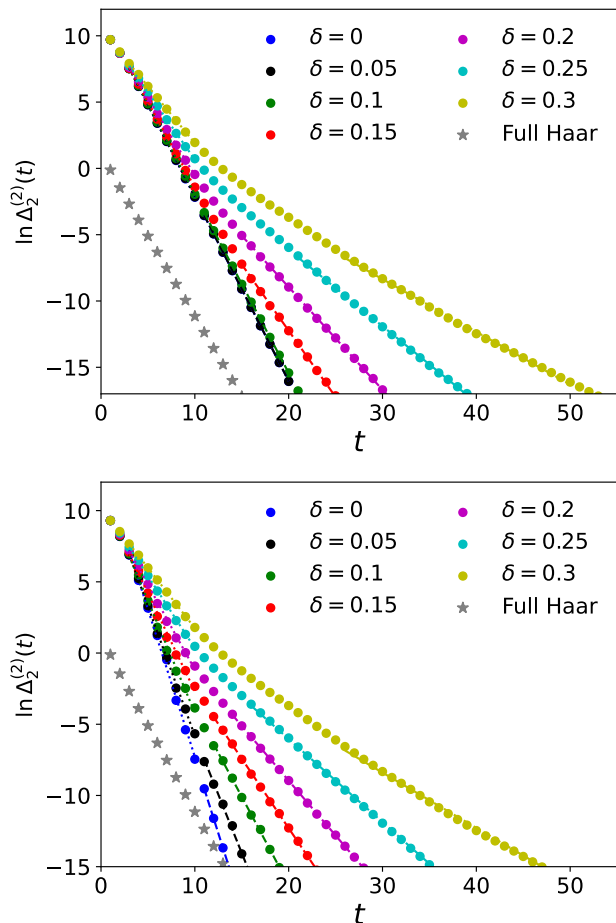


FIG. 4. Calculating $\Delta_2^{(2)}(t)$ with explicit averaging for various δ . All data is from system size $L = 4$ (8 qubits). (Top) Boundary randomness is random Pauli matrices [Case (a.1)]. (Bottom) Boundary randomness is with one site Haar random unitaries [Case (a.2)].

First we note that the two step relaxation of Eq. (19) is only observed for small entangling power $p < 0.4$ in Fig. 7. For large p we instead see a state dependent relaxation prior to settling into an exponential decay with a roughly p independent rate. We report the fits for the decay rates in Tab. I. For comparison, the decay rate in Eq. (22) of the Haar random brickwork circuit for $d = 2$ gives $r_2^{(2)} \approx 0.89257$. The small entangling power $p = 0.2$ has a similar decay rate to the Haar random brickwork circuit, while the cases tested with higher entangling power $p \geq 0.3$ decay significantly faster.

Next we move away from the DU point but continue to perform averaging as prescribed in Case (b.1). To do this we return to the parameterisation in Eq. (13). We fix $J = 0.1$ and vary δ . This is shown in the bottom plot of Fig. 7. Again we only see the two step relaxation as defined in Eq. (19) for small p and a state dependent short time regime for larger p . The second decay regime is observed for all p , and $r_2^{(2)}$ is reported in Tab. I. We note that the

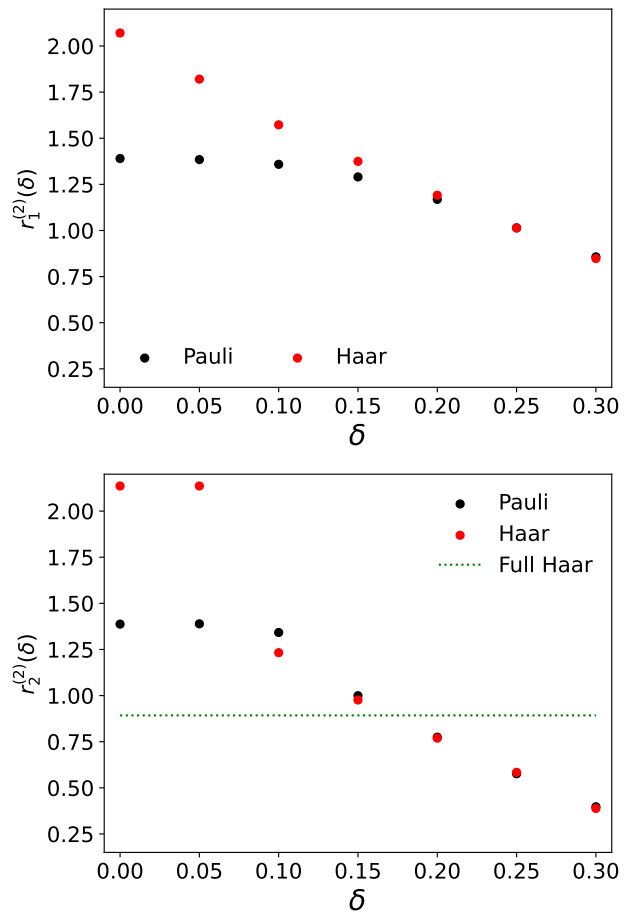


FIG. 5. $r_1^{(2)}, r_2^{(2)}$ for various δ from the $L = 4$ data presented in Fig. 4. The full Haar value is calculated for $d = 2$ in Eq. (22).

correlation between p and the decay rate is weaker than in the DU case. For example, in Fig. 7 we have two points with similar entangling power $p \approx 0.64$ and $p \approx 0.63$ and visibly different decay rates. When the entangling power is similar, gates that are closer to the DU point appear to generate an appreciably faster decay (we have respectively $\delta = 0.1$ and $\delta = 0.2$ in the aforementioned example). Moreover, for non-DU averaged gates we see that more entangling power is necessary to be as fast as the Haar random case result with $p \approx 0.59$ giving us a result similar to the Haar rate given in Eq. (22). For higher entangling power, however, we observe rates significantly faster than Haar random.

Finally, we also consider $k = 3$. Specifically, in Fig. 8 we report the dynamics of $\Delta_2^{(k=3)}(t)$ for three static gate choices. In this case we can reach a maximum system size of $2L = 10$ by embedding our effective Hilbert space dimension of 6 permutation states inside 8 qubits. Due to system size constraints we only witness early time state-dependent dynamics, however, we see quick convergence of the 3-moments to the Haar value.

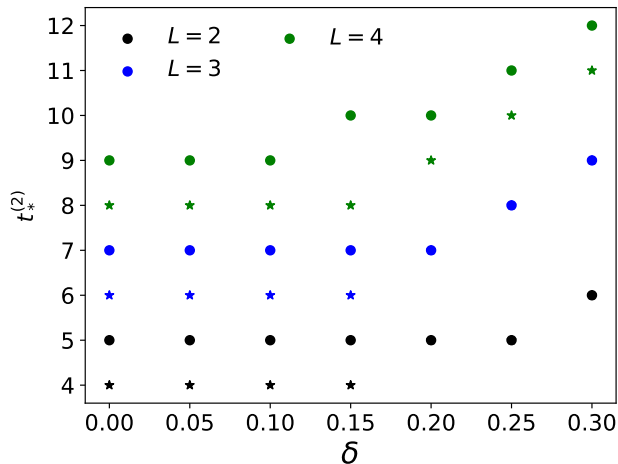


FIG. 6. $t_*^{(2)}$ as a function of δ , extracted from data given in the figures in Fig. 4 and similar data sets for $L = 2, 3$. $t_*^{(2)}$ is extracted as the first point incompatible with the first decay regime. Solid circle are from Case (a.1) and stars are Case (a.2).

DU		Non-DU	
p	$r_2^{(2)}$	p	$r_2^{(2)}$
0.1	0.41	0.18	0.12
0.2	0.85	0.34	0.25
0.3	1.39	0.49	0.50
0.4	2.10	0.59	0.86
0.5	2.74	0.63	1.40
0.6	2.77	0.64	2.00
0.7	2.73		
0.8	2.77		

TABLE I. Decay rates for different entangling power p , extracted from both plots in Fig. 7 in Case (b.1).

IV. ANALYSIS

Let us now provide an analytical characterisation of the behaviours discussed in the previous section. We begin by introducing a theoretical framework to approach the problem and discuss some general features — including the rigorous statement on the production of quantum state k -designs at sufficiently large times. We then specialise the treatment to the case where the local gates in Eq. (1) are DU, this allows us to obtain further analytical results supporting our interpretations.

Since the settings of interest in this work (cf. Sec. II) involve quantum circuits with randomness without time correlations, the time evolution of $\rho_t^{(k)}$ (cf. Eq. (7)) is *Markovian*, i.e., the k -moment at time $t+1$ only depends on that at time t . More precisely we have

$$\rho_{t+1}^{(k)} = \mathcal{B}_k[\rho_t^{(k)}], \quad (24)$$

where we introduced the linear super operator \mathcal{B}_k :

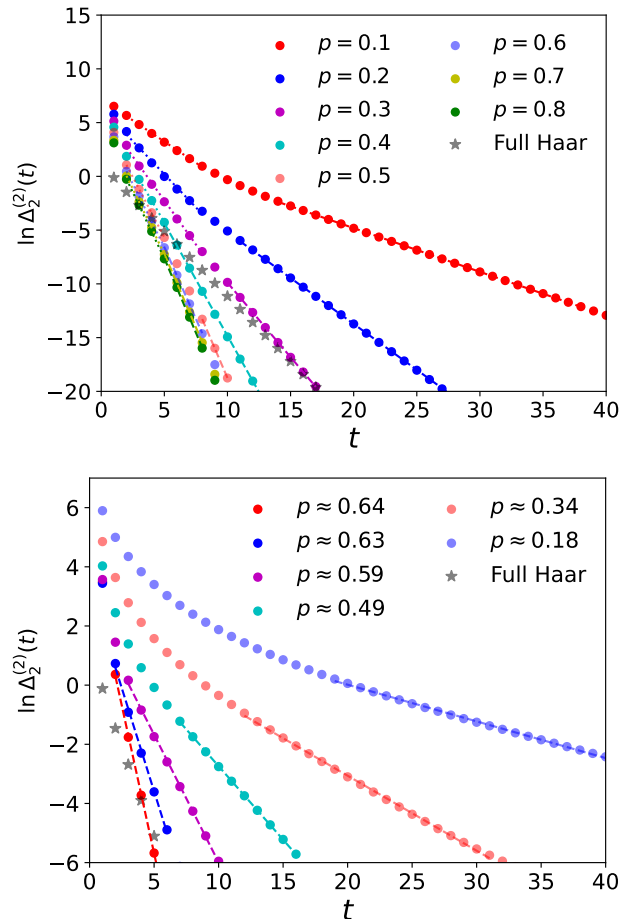


FIG. 7. Calculating $\Delta_2^{(2)}(t)$ with explicit averaging over Case (b.1) circuits. (Top) Dynamics generated by DU gates defined in Eq. (63) for $L = 14$ and $k = 2$. We set $d = 2$ for this example. (Bottom) Non-DU gates using the parametrization of Eq. (13). We set $J = 0.1$ and vary δ . In the figure we report the entangling power p of the averaged gate, which corresponds to (from high to low entangling power) an evenly spaced set of $\delta = 0.1 \dots 0.6$. Here $L = 14$ as well.

$\text{End}(\mathbb{C}^{d^{2kL}}) \rightarrow \text{End}(\mathbb{C}^{d^{2kL}})$ defined by

$$\mathcal{B}_k[A] = \sum_{\vec{\alpha}_t \in S} \mathcal{U}(\vec{\alpha}_t) A \mathcal{U}^\dagger(\vec{\alpha}_t) \quad A \in \text{End}(\mathbb{C}^{d^{2kL}}). \quad (25)$$

As it is apparent from its definition — $\mathcal{B}_k[\cdot]$ is written in Krauss form with unitary Krauss operators — this super operator is a unital and trace preserving quantum channel, i.e., a unital CPTP map [43]. This map is non-expanding, i.e., its spectrum lies on the unit disk of the complex plane.

An analysis of the fixed points of this channel allows us to answer a basic question about k -designs generation in the settings under exam. Indeed, straightforwardly adapting a theorem by Ippoliti and Ho (cf. Sec. 3 C of Ref. [26]), we can show that for almost all choices of two-site gates, the brickwork circuit in Eq. (1) does indeed produce quantum state k -designs for sufficiently large

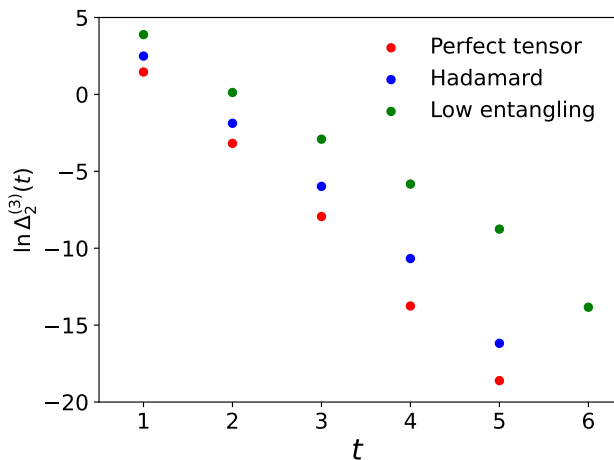


FIG. 8. Time-dependence of $\Delta_2^{(3)}(t)$ for three instances of Case (b.1). The non-random 2-qudit gate in Eq. (4) is taken to be either a perfect tensor, cf. Eqs. (81–83) (red), a Hadamard gate $U_{cd}^{ab} = \delta_{a,d}\delta_{b,c} \exp(i2\pi ab/d)$ (blue), or a dual-unitary gate of the form $U_{cd}^{ab} = \delta_{a,d}\delta_{b,c} \exp(iJ_{ab})$ (green). In the simulations we set $d = 3$, and chose $(J_{00}, J_{01}, \dots, J_{22}) = (6.03, 4.24, 2.86, 5.68, 5.84, 1.34, 4.44, 3.51, 2.62)$.

times. More precisely, denoting by $\mathcal{A}_V \subset U(d)$ the open set containing $V \in U(d)$, we have the following rigorous statement

Property 1. *For all the three Cases (a.1), (a.2), and (b.1) the limit state*

$$\lim_{t \rightarrow \infty} \rho_t^{(k)} = \rho_\infty^{(k)}, \quad (26)$$

exists and — for almost all $\{U^{(n)}\} \in \mathcal{A}_V$ (cf. Eq. (1)) and any (\mathcal{A}_V, V) — $\rho_\infty^{(k)} = \rho_H^{(k)}$.

This statement guarantees that in all three Cases (a.1), (a.2), and (b.1), choosing $\{U^{(n)}\}$ in the arbitrary open set \mathcal{A}_V , we almost always produce a circuit that generates the Haar distribution at large enough times, confirming our numerical observations of the previous section. Note that, crucially, no averaging is performed over the $\{U^{(n)}\}$. See App. A for a proof of this statement.

Our second question — concerning the way in which the Haar distribution is approached — is instead more difficult to answer. To make some progress we apply the standard vectorisation (folding) mapping

$$|i\rangle\langle j| \mapsto |i, j\rangle, \quad (27)$$

where $\{|j\rangle, j = 1, \dots, d\}$ is the local computational basis. Then we can represent $\mathcal{B}_k[\cdot]$ as a matrix in $\text{End}(\mathbb{C}^{d^{4kL}})$. For brevity, we make a little abuse of notation and denote the matrix corresponding to $\mathcal{B}_k[\cdot]$ with the same symbol but remove the explicit dependence on the input, i.e., we write it as \mathcal{B}_k . The matrix \mathcal{B}_k inherits the spectral properties of the channel $\mathcal{B}_k[\cdot]$. Namely, labelling its eigenvalues as $\{\lambda_{m,q}\}$ we have $|\lambda_{m,q}| \leq 1$. In this labelling

m ranks the eigenvalues magnitude in descending order, $|\lambda_{m,q}| > |\lambda_{m+1,q}|$, and q distinguishes eigenvalues with degenerate magnitudes, $|\lambda_{m,q+1}| = |\lambda_{m,q}| \equiv |\lambda_m|$ [44]. Instead, we represent the vectorised form of $\rho_t^{(k)}$ as $|\rho_t^{(k)}\rangle$. Note that

$$|\rho_0^{(k)}\rangle = (|\psi\rangle \otimes |\psi\rangle^*)^{\otimes k}, \quad (28)$$

where $|\psi\rangle$ is the initial state (cf. Sec. II).

Putting everything together, we can represent the vectorised k -moment at time t as

$$|\rho_t^{(k)}\rangle = \mathcal{B}_k^t |\rho_0^{(k)}\rangle = \sum_{m \geq 0} \sum_{q=0}^{p_m-1} \lambda_{m,q}^t c_{m,q}^{(l)} |\lambda_{m,q}^{(r)}\rangle, \quad (29)$$

where $|\lambda_{m,q}^{(r)}\rangle$ ($\langle\lambda_{m,q}^{(l)}|$) is the right (left) eigenvector associated to $\lambda_{m,q}$, p_m denotes the degeneracy of $|\lambda_{m,q}|$, and we set

$$c_{m,q}^{(l)} = \langle\lambda_{m,q}^{(l)}|\rho_0^{(k)}\rangle, \quad c_{m,q}^{(r)} = \langle\rho_0^{(k)}|\lambda_{m,q}^{(r)}\rangle. \quad (30)$$

Property 1 ensures that the eigenspace associated with the maximal-magnitude eigenvalue $\lambda_0 = 1$ produces the vectorised form of the k -th moment of the Haar ensemble in all the three cases considered here (a.1). More precisely

$$|\rho_H^{(k)}\rangle = \sum_{q=0}^{p_0-1} c_{0,q}^{(l)} |\lambda_{0,q}^{(r)}\rangle, \quad \langle\rho_H^{(k)}| = \sum_{q=0}^{p_0-1} c_{0,q}^{(r)} \langle\lambda_{0,q}^{(l)}|. \quad (31)$$

Therefore, Eq. (29) can be re-written as

$$|\rho_t^{(k)}\rangle - |\rho_H^{(k)}\rangle = \sum_{m=1}^{p_0-1} \sum_{q=0}^{p_m-1} \lambda_{m,q}^t c_{m,q}^{(l)} |\lambda_{m,q}^{(r)}\rangle, \quad (32)$$

which gives

$$\begin{aligned} \|\rho_t^{(k)} - \rho_H^{(k)}\|_2^2 &= \|\rho_t^{(k)}\rangle - |\rho_H^{(k)}\rangle\|_2^2 \\ &= \sum_{m,m' \geq 1} \sum_{q,q'=0}^{p_m-1} \lambda_{m,q}^t (\lambda_{m',q'}^*)^t c_{m,q}^{(l)} c_{m',q'}^{(l)*} \langle\lambda_{m',q'}^{(r)}|\lambda_{m,q}^{(r)}\rangle, \end{aligned} \quad (33)$$

where we used that the Frobenius norm becomes the standard vector norm upon vectorisation.

This expression immediately implies that in the regime $t \gg L$ the time-evolution of $\|\rho_t^{(k)} - \rho_H^{(k)}\|_2^2$ — and hence of $\Delta_2^{(k)}(t)$ in Eq. (9) — is entirely determined by the magnitude of the leading sub-leading eigenvalue of the matrix \mathcal{B}_k . Namely

$$\Delta_2^{(k)}(t) \simeq \frac{C}{k!} |\lambda_1|^{2t} d^{2kL}, \quad t \gg L \gg 1, \quad (34)$$

where we used Stirling's approximation for the Haar moments in Eq. (12). Note that $|\lambda_1|$ bears an implicit dependence on k and L but it typically saturates to a finite

constant value $|\bar{\lambda}_1| < 1$ at large L . In this case one obtains ϵ -approximate k -designs in a time

$$\tau_k^{(\epsilon)} \simeq \frac{1}{2 \ln(1/|\bar{\lambda}_1|)} (2kL \ln d - \log \epsilon), \quad (35)$$

where we neglected $O(1)$ contributions. This is the same leading-order scaling expected for Haar random circuits [12].

Eq. (34) does not automatically apply in the regime $1 \ll t \ll L$, where the contribution of the higher terms in Eq. (33) is not necessarily suppressed and can change the scaling with t . This can lead $\Delta_2^{(k)}(t)$ to show an exponential decay with a different exponent $r_1^{(k)} \neq 2 \ln |\lambda_1|$ similarly to what observed in the other accounts of two-step relaxation [30–34, 36]. Below we consider the case of minimally random circuits of DU gates where this phenomenology can be (partially) shown to occur. We also argue that in dual-unitary circuits with high enough entangling power $|\lambda_1|$ is smaller than for fully Haar random circuits, implying that the former generate random states faster than the Haar random case.

A. Dual unitary gates: Case (a)

Let us now assume that our two-local gates are DU, and focus on Case (a). For convenience, we assume the initial state to be a product of (generalised) Bell pairs

$$|\psi\rangle = \left(\frac{1}{\sqrt{d}} \sum_{j=1}^d |j, j\rangle \right)^{\otimes L}, \quad (36)$$

where d is the local Hilbert space dimension. The reason for this choice — which contrasts with the product states used elsewhere in this manuscript — is that they belong to the class of *solvable* initial states [45, 46], which allows us to completely characterise the frame potential $F_t^{(k)}$ whenever $t < 2L$.

We start by introducing the diagrammatic tensor-network notation, where a node with an open leg represents a vector in the space $\mathbb{C}^{d^{2k}}$, and a node with a number of outgoing legs is a vector (or a matrix/more general tensor) in the tensor product of a number of local spaces determined by the number of legs. In particular, we represent the local time-evolution operator acting on $\mathbb{C}^{d^{2k}} \otimes \mathbb{C}^{d^{2k}}$ with square boxes

$$\boxed{k} = (U \otimes U^*)^{\otimes k}, \quad \boxed{k}^\dagger = \boxed{k}^\dagger = (U^\dagger \otimes U^T)^{\otimes k}, \quad (37)$$

where \otimes represents the tensor product in the replicated space. Similarly, we represent with a circle the average over randomly chosen one-site unitaries

$$\mathcal{D}_k = \oint_k = \oint_k^\dagger = \sum_{\alpha \in \mathcal{S}} \mu_S(\alpha) (\alpha \otimes \alpha^*)^{\otimes k}. \quad (38)$$

Using the convention that connected lines represent index summation, we can now express the time-evolution operator \mathcal{B}_k as

$$\mathcal{B}_k = \overbrace{\left(\boxed{k} \right)}^L, \quad (39)$$

where L denotes the number of pairs of open legs ($L = 5$ in the above example), while the initial state $|\rho_0^{(k)}\rangle$ is diagrammatically given as

$$|\rho_0^{(k)}\rangle = \frac{1}{d^{kL}} \underbrace{\left(\right)}_L. \quad (40)$$

Using this we can express the frame potential

$$F_t^{(k)} = \langle \rho_t^{(k)} | \rho_t^{(k)} \rangle = \langle \rho_0^{(k)} | \mathcal{B}_k^{\dagger t} \mathcal{B}_k^t | \rho_0^{(k)} \rangle \quad (41)$$

with the left diagram in Fig. 9. The diagram is simplified by taking into account the fact that U is unitary, $UU^\dagger = U^\dagger U = \mathbb{1}$, which gives the following diagrammatic relation

$$\left(\boxed{k} \right) = \left(\right). \quad (42)$$

Repeatedly applying this to the l.h.s. of Fig. 9 and assuming $t < L$, we obtain two connected triangular tensor networks scaling with t , as shown in the middle panel of Fig. 9.

Note that up to this point we have not used any special property of our gates. As anticipated before, however, here we are interested in a special family of gates characterised by the *dual-unitarity* property. Namely, we consider gates that are unitary also when propagating in space. More concretely, we consider gates for which the space-time dual matrix \tilde{U} with the matrix elements give by

$$\langle s_1 s_2 | \tilde{U} | s_3 s_4 \rangle = \langle s_1 s_3 | U | s_2 s_4 \rangle, \quad (43)$$

is unitary, i.e.

$$\tilde{U}^\dagger \tilde{U} = \tilde{U} \tilde{U}^\dagger = \mathbb{1}. \quad (44)$$

Graphically, this implies that a box factorises into two lines also when it is connected with its Hermitian conjugate from the side

$$\left(\boxed{k} \right) = \left(\right). \quad (45)$$

Repeatedly applying the dual-unitarity condition to the middle-panel of Fig. 9, we obtain the right-most panel, which reads explicitly as

$$F_t^{(k)} = (d^{-2k} \text{tr}[\mathcal{D}_k^2])^t. \quad (46)$$

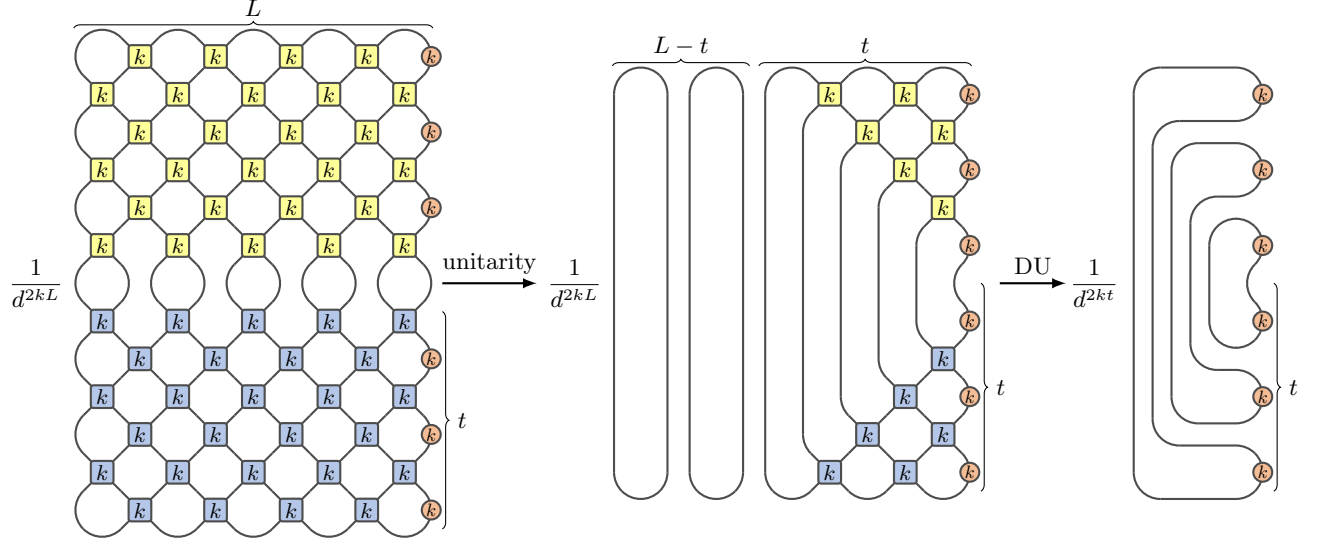


FIG. 9. Diagrammatic representation of $F_t^{(k)}$ for $t \leq L$ and dual unitary gates. Using the unitarity condition (42), the diagram simplifies into the middle panel, while the factorised result in the right-most panel follows from additional application of dual unitary condition (45).

This expression clearly depends on the choice of boundary driving confirming our observation of Sec. III. In particular, evaluating Eq. (46) in Case (a.1), we can see that there is no k -dependence

$$F_t^{(k)} \Big|_{(a.1)} = 4^{-t}, \quad (47)$$

while in Case (a.2) the frame potential reduces to the average of powers of trace of $d \times d$ random unitaries

$$F_t^{(k)} \Big|_{(a.2)} = (d^{-2k} T_{d,k})^t, \quad T_{d,k} = \int_{U(d)} dU |\text{tr}[U]|^{2k}, \quad (48)$$

which for generic d and k takes the following form [47]

$$T_{d,k} = k!^2 \sum_{l=1}^d \sum_{\substack{s_1 + \dots + s_l = k \\ s_1 \geq s_2 \geq \dots \geq s_l}} \frac{\prod_{i=1}^{l-1} \prod_{j=i+1}^l (s_i - s_j - i + j)^2}{\prod_{i=1}^l (l - i + s_i)!^2}. \quad (49)$$

Note that in the case of $d = 2$, the above expression reduces to the k -th Catalan number C_k ,

$$T_{2,k} = \frac{1}{k} \binom{2k}{k-1} \equiv C_k, \quad (50)$$

while for $d > k$ we have [47],

$$T_{d \geq k,k} = k!. \quad (51)$$

This fully characterises the initial decay regime (i.e. $t < L$), giving us

$$r_1^{(k)} = \begin{cases} 2 \ln 2, & \text{(a.1),} \\ 2k \ln 2 - \ln C_k, & \text{(a.2), } d = 2, \\ 2k \ln d - \ln T_{d,k}, & \text{(a.2), arbitrary } d. \end{cases} \quad (52)$$

This is consistent with Fig. 1, where the initial decay for Case (a.1) is independent of k , and it reproduces the $d = k = 2$ decay rate in Fig. 4 for (a.2). For qubits we immediately observe that for an arbitrary $k \geq 1$ we have

$$r_1^{(k)} \Big|_{(a.2), d=2} \geq r_1^{(1)} \Big|_{(a.2), d=2} = r_1^{(k)} \Big|_{(a.1)}. \quad (53)$$

Note that for $k = 1$, we can simplify the diagram in Fig. 9 for any time as \mathcal{D}_1 becomes a projector

$$\mathcal{D}_1 = |\mathcal{O}_1\rangle\langle\mathcal{O}_1|, \quad (54)$$

where $|\mathcal{O}_1\rangle$ denotes a (normalised) vectorised identity operator

$$|\mathcal{O}_1\rangle = \frac{1}{\sqrt{d}} \sum_{j=1}^d |jj\rangle. \quad (55)$$

Graphically, we represent Eq. (54) as

$$\text{⊙} = \text{⊙}. \quad (56)$$

Furthermore, the unitarity of U implies

$$\text{⊠} = \text{⊙}, \quad \text{⊠} = \text{⊙}, \quad (57)$$

while the dual-unitary condition gives,

$$\text{⊠} = \text{⊙}, \quad \text{⊠} = \text{⊙}. \quad (58)$$

Considering now the diagram on the l.h.s. of Fig. 9 for $t > L$, we can first replace the dissipators \mathcal{D}_1 with the projector to $|\mathcal{O}_1\rangle$, and then repeatedly apply Eq. (58),

and (57) to completely factorise the diagram obtaining d^{-2L} . Combining it with the result for $t \leq L$ we therefore have

$$F_t^{(1)} = \begin{cases} d^{-2t}, & t \leq L, \\ d^{-2L}, & t > L. \end{cases} \quad (59)$$

Instead, for general $k > 1$ dual-unitarity does not lead to direct simplifications when time is large compared to the system size. This is expected, as in this regime the dual-unitary dynamics are BQP-complete [48]. To gain more analytical insight, we therefore increase the amount of randomness, and consider Case (b).

B. Dual unitary gates: Case (b)

Let us now consider Case (b) for dual unitary gates. We begin by focusing on $k = 2$ and then move to $k > 2$. The time-evolution operator \mathcal{B}_2 now consists of averaged gates W , which can be understood as the blue gates in Eq. (37), decorated with one-site projectors \mathcal{D}_2

$$W = \begin{array}{c} \textcircled{2} \\ \text{---} \\ \textcircled{2} \end{array} = \begin{array}{c} \textcircled{2} \quad \textcircled{2} \\ \diagdown \quad \diagup \\ \textcircled{2} \quad \textcircled{2} \end{array}. \quad (60)$$

This gives the following diagrammatic expression for \mathcal{B}_2

$$\mathcal{B}_2 = \overbrace{\begin{array}{c} \textcircled{2} \quad \textcircled{2} \quad \textcircled{2} \quad \textcircled{2} \quad \textcircled{2} \\ \diagdown \quad \diagup \quad \diagdown \quad \diagup \quad \diagdown \quad \diagup \\ \textcircled{2} \quad \textcircled{2} \quad \textcircled{2} \quad \textcircled{2} \quad \textcircled{2} \end{array}}^L. \quad (61)$$

The averaged gate W is projected to the subspace spanned by $|\textcircled{O}\rangle$ and $|\square\rangle$ defined as

$$\begin{aligned} |\textcircled{O}\rangle &= \frac{1}{d} \sum_{s_1, r_1, s_2, r_2} \delta_{s_1, r_1} \delta_{s_2, r_2} |s_1, r_1, s_2, r_2\rangle, \\ |\square\rangle &= \frac{1}{d} \sum_{s_1, r_1, s_2, r_2} \delta_{s_1, r_2} \delta_{s_2, r_1} |s_1, r_1, s_2, r_2\rangle, \\ |\bullet\rangle &= \frac{d|\square\rangle - |\textcircled{O}\rangle}{\sqrt{d^2 - 1}}, \end{aligned} \quad (62)$$

and takes the following form in the (orthonormal) basis of $\{|\textcircled{O}\rangle, |\bullet\rangle\}$ [49]

$$W = \begin{bmatrix} 1 & 0 & 0 & 0 \\ 0 & 0 & 1-p & \frac{p}{\sqrt{d^2-1}} \\ 0 & 1-p & 0 & \frac{p}{\sqrt{d^2-1}} \\ 0 & \frac{p}{\sqrt{d^2-1}} & \frac{p}{\sqrt{d^2-1}} & 1 - \frac{2p}{d^2-1} \end{bmatrix}. \quad (63)$$

Here the free parameter p is the entangling power [49–53], defined as the average linear entropy generated by the gate when acting on Haar-random product states. In particular, for a DU gates acting on qubits it can be expressed as [54]

$$p = \frac{2}{3} \cos(2J)^2, \quad (64)$$

where J is the parameter of the dual-unitary gate appearing in Eq. (13).

1. Late-time regime

Let us first consider times t that are large compared to the system size L . In this regime the dynamics of $|\rho_t^{(2)}\rangle$ is governed by the leading subleading eigenvalue of \mathcal{B}_2 . First let us note that both $|\textcircled{O}\textcircled{O}\rangle$ and $|\square\square\rangle$ are invariant under the action of W , which implies that \mathcal{B}_2 has two eigenvectors corresponding to eigenvalue 1: $|\textcircled{O}\rangle^{\otimes 2L}$ and $|\square\rangle^{\otimes 2L}$. Property 1 guarantees that the latter are the only ones.

To find the subleading eigenvalue λ_1 , let us start by defining projectors P_1 and P_2 to the subspaces $\mathcal{V}_{1,2}$ defined as

$$\begin{aligned} \mathcal{V}_1 &= \text{Span}\{|\textcircled{O}\rangle^{\otimes j} \otimes |\square\rangle^{\otimes 2L-j}\}_{j=1}^{2L-1}, \\ \mathcal{V}_2 &= \text{Span}(\{|\textcircled{O}\rangle^{\otimes j} \otimes |\bullet\rangle \otimes |\textcircled{O}\rangle^{\otimes 2L-j-1}\}_{j=0}^{2L-1}). \end{aligned} \quad (65)$$

Even though the projectors $P_{1,2}$ do not commute with \mathcal{B}_2 (and are not orthogonal) Ref. [36] has argued that the dominant subleading eigenvalues of \mathcal{B}_2 are well approximated by either the leading spectrum of $P_1\mathcal{B}_2P_1$ or $P_2\mathcal{B}_2P_2$. This is based on an entanglement membrane approach [55, 56] supplemented with the observation that structured random unitary circuits support ‘magnon excitations’. While the membrane approach suggests that \mathcal{V}_1 should contain the leading eigenvectors, the presence of magnons indicates that also \mathcal{V}_2 should play a role. This competition led Ref. [36] to argue that the value of $|\lambda_1|$ is determined as the largest of the eigenvalues of the two blocks. The first one is found to be d^{-2} [56], while the second is the square of the leading eigenvalue of the channel

$$\begin{array}{c} \textcircled{2} \\ \diagdown \quad \diagup \\ \textcircled{2} \end{array}, \quad (66)$$

which turns out to be $(1-p)^2$. This gives

$$|\lambda_1| \approx \max\{d^{-2}, (1-p)^2\}. \quad (67)$$

This prediction is expected to hold in the limit of large L , but as we see from numerical test in Fig. 10, it works well already for moderate system sizes. For sufficiently entangling circuits ($p \geq 1 - 1/d$) we therefore expect $|\lambda_1| \approx d^{-2}$ and

$$\Delta_2^{(2)} \sim d^{4(L-t)}, \quad (68)$$

for $t \gg 2L$. Recalling Eq. (35) this gives an ϵ -approximate 2-design in a time

$$\tau_2^{(\epsilon)} \simeq L - \frac{\log \epsilon}{4 \ln(d)}, \quad (69)$$

which we argue is the shortest possible in brickwork circuit.

2. Early-time regime

Let us now examine the case in which time is short compared to the system size, more precisely, $L \geq 2t$.

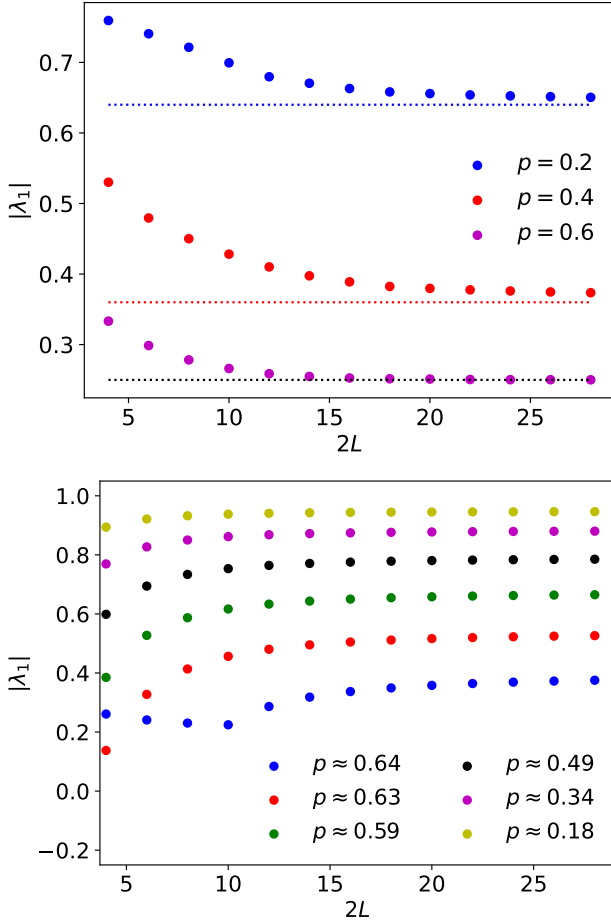


FIG. 10. $|\lambda_1|$ for $k = 2$. (Top) $|\lambda_1|$ for the Case (b) circuit filled with average DU gates. All data here is for $d = 2$. Horizontal line corresponds to (67). (Bottom) $|\lambda_1|$ for Case (b) circuits away from the DU point. Data from the circuit defined for bottom plot of Fig. 7.

In this case we expect to see no contribution from the subspace \mathcal{V}_2 . To see this, consider the overlap between a vector from \mathcal{V}_2 and $|\rho_t^{(2)}\rangle$

$$O_{x,t} = \langle \underbrace{\text{O}_2 \dots \text{O}_2}_x \bullet_2 \underbrace{\text{O}_2 \dots \text{O}_2}_{2L-x-1} |\rho_t^{(2)}\rangle. \quad (70)$$

Setting the initial state $|\rho_0^{(2)}\rangle$ to be a product of pairs as in Eq. (40), we can express the overlap diagrammatically as

$$O_{x,t} = \frac{1}{d^{4L}} \left(\begin{array}{c} \overbrace{\text{O}_2 \dots \text{O}_2}^{\lfloor \frac{x}{2} \rfloor} \bullet_2 \overbrace{\text{O}_2 \dots \text{O}_2}^{\lfloor \frac{2L-x-1}{2} \rfloor} \\ \text{Diagrammatic representation of the overlap} \end{array} \right) \cdot t \quad (71)$$

The diagram can be simplifying by noting that $|\text{OO}\rangle$ is invariant under W , which is diagrammatically expressed as

$$\boxed{2} = \text{O} \text{O}, \quad \boxed{2} = \text{O} \text{O}, \quad (72)$$

and observing that the dual unitarity of the original gate gives the following two additional relations satisfied by W

$$\boxed{2} = \text{O} \text{O}, \quad \boxed{2} = \text{O} \text{O}. \quad (73)$$

This immediately gives

$$O_{j,t} |_{j \geq 2t \text{ or } j < 2(L-t)} = \langle \bullet_2 | \text{O}_2 \rangle = 0. \quad (74)$$

Thus whenever $L \geq 2t$ the sector corresponding to the subspace \mathcal{V}_2 cannot contribute to the decay of $\Delta_2^{(2)}$ and for large t we asymptotically expect

$$\Delta_2^{(2)} \Big|_{t \leq L/2} \sim d^{-2t}. \quad (75)$$

In the case $(1-p)^2 > d^{-2}$ then we expect to see the relaxation with two different slopes, first $4 \log d$ and then $-4 \log(1-p)$. Instead for $(1-p)^2 \geq d^{-2}$ we expect $\Delta_2^{(2)}$ to decay as d^{-4t} in both time regimes and for all entangling powers above the threshold. This is in agreement with the numerical findings reported in Fig. 7.

3. Higher designs: $k > 2$

The main insight of Ref. [36], i.e., that the leading sub-leading eigenvalue of \mathcal{B}_2 is given by either the ‘magnon configurations’ or the domain walls (cf. Sec. IV B 1), is not limited to $k = 2$ and can be applied to arbitrary designs $k > 2$. Namely, to find the leading sub-leading eigenvalue of

$$\mathcal{B}_k = \overbrace{\left(\begin{array}{c} \text{Diagrammatic representation of } \mathcal{B}_k \end{array} \right)}^L, \quad (76)$$

where we introduced

$$\boxed{k} = \begin{array}{c} \text{Diagrammatic representation of } \boxed{k} \end{array}. \quad (77)$$

The main additional difficulties occurring in the general case are two: (i) the domain wall subspace \mathcal{V}_1 is more complicated and involves domain walls among any possible ‘permutation states’ $|\sigma_j\rangle$, defined by the following matrix elements in the computational basis of $2k$ qudits $(|s_1 r_1 \dots s_k r_k\rangle_{s_j, r_j=1}^d)$

$$\langle s_1 r_1 \dots s_k r_k | \sigma_j \rangle = \prod_{m=1}^k \delta_{s_m, r_{\sigma(m)}}. \quad (78)$$

(ii) the leading eigenvalue, ρ_k , in the magnon subspace \mathcal{V}_2 , which was determined in Ref. [36] as the leading sub-leading eigenvalue of

$$\begin{array}{c} \circ \\ | \\ \boxed{k} \\ | \\ \circ \end{array}, \quad (79)$$

squared, is not just given by $(1-p)^2$.

In a random DU circuit, however, it is still true that the leading eigenvalue of $P_1 \mathcal{B}_2 P_1$ continues to be asymptotically given by d^{-2} [56]. Therefore Eq. (67) should be replaced by

$$|\lambda_1| \approx \max\{d^{-2}, \rho_k\}. \quad (80)$$

This equation suggests that the family of DU circuits with the fastest speed of k -design preparation should depend on k . In fact, since one can easily show that $\rho_k \geq (1-p)^2$, this family should shrink by increasing k . Finding the explicit k dependence is difficult as there is no general way to determine ρ_k analytically for arbitrary values of k . The latter, however, can be found for certain specific classes of DU gates. For example, considering *perfect tensors* [57–61] that, besides the dual-unitarity conditions

$$\begin{array}{c} \circ \\ | \\ \boxed{k} \\ | \\ \circ \end{array} = \begin{array}{c} \circ \\ | \\ \circ \end{array} \begin{array}{c} \circ \\ | \\ \circ \end{array}, \quad \begin{array}{c} \circ \\ | \\ \boxed{k} \\ | \\ \circ \end{array} = \begin{array}{c} \circ \\ | \\ \circ \end{array} \begin{array}{c} \circ \\ | \\ \circ \end{array}, \quad (81)$$

and

$$\begin{array}{c} \circ \\ | \\ \boxed{k} \\ | \\ \circ \end{array} = \begin{array}{c} \circ \\ | \\ \circ \end{array} \begin{array}{c} \circ \\ | \\ \circ \end{array}, \quad \begin{array}{c} \circ \\ | \\ \boxed{k} \\ | \\ \circ \end{array} = \begin{array}{c} \circ \\ | \\ \circ \end{array} \begin{array}{c} \circ \\ | \\ \circ \end{array}, \quad (82)$$

also fulfil

$$\begin{array}{c} \circ \\ | \\ \boxed{k} \\ | \\ \circ \end{array} = \begin{array}{c} \circ \\ | \\ \circ \end{array} \begin{array}{c} \circ \\ | \\ \circ \end{array}, \quad \begin{array}{c} \circ \\ | \\ \boxed{k} \\ | \\ \circ \end{array} = \begin{array}{c} \circ \\ | \\ \circ \end{array} \begin{array}{c} \circ \\ | \\ \circ \end{array}, \quad (83)$$

one immediately has $\rho_k = 0$ (and also $p = 1$). Tensors fulfilling these properties do not exist for $d = 2$ but are known to exist for any $d \geq 3$ [62, 63]. As a result, for perfect tensors one expects the same (maximally fast) decay in time for all $\Delta_2^{(k)}$, i.e.,

$$\Delta_2^{(k)} \sim \frac{C}{k!} d^{2kL} d^{-4t}, \quad \forall k. \quad (84)$$

For large L and fixed k this gives

$$\tau_k^{(\epsilon)} \simeq \frac{k}{2} L - \frac{\log \epsilon}{4 \ln(d)}, \quad (85)$$

which we argue is the shortest time to achieve an ϵ -approximate k design with a brickwork quantum circuit.

As for the $k = 2$ case, Eq. (80) seems in good agreement with our numerical calculations also for $k = 3$, see Tab. II. This is remarkable given the fact that the accessible values of L are substantially smaller in this case than for $k = 2$.

L	2	3	4	5
Perfect tensor	0.125	0.114574	0.111721	0.111124
Hadamard	0.170067	0.138011	0.123132	0.116489
Low entangling	0.369653	0.322775	0.286805	0.26456

TABLE II. Dominant subleading eigenvalue $|\lambda_1|$ for selected average DU models and $k = 3$ and $d = 3$. The gate definitions can be found in the caption of Fig. 8. For these three cases we have $\rho_3 = 0$, $\rho_3 = 0.125$, and $\rho_3 = 0.224776$ respectively. In these three cases we also have $\rho_3 = (1-p)^2$. The value λ_1 was obtained from a hybrid subspace iteration method to isolate the leading eigen-pairs with $\lambda_{0,q} = 1$, followed by an Arnoldi method to isolate $\lambda_{1,q}$. In the low entangling case for $L = 5$ the convergence criteria were not met and we report the final eigenvalue magnitude estimate.

V. CONCLUSIONS

In this work we investigated quantum-state-design preparation in local quantum circuits with a minimal degree of randomness. We considered two cases, both in the framework of brickwork circuits of finite size: (a) fixed circuits with a single one-qudit random unitary matrix at the boundary; (b) brickwork circuits with one-qudit random unitary matrices everywhere but fixed interactions. Both cases are characterised by the property that the entangling part of the local gate is *not* random.

We found that both these settings produce quantum state designs for sufficiently large depths. In fact, if the local gates are sufficiently entangling, they do so *faster* than fully random (Haar random) brickwork circuits. More specifically, we found that if the local gates are dual-unitary there is a direct relationship between the speed of 2-design preparation and the entangling power [50–53] of the local gates. The speed of 2-design preparation grows monotonically with the entangling power for small values of the latter, and, above a critical value, it saturates to its maximal value — this is a crossover for finite width but approaches a phase transition in the limit of infinite width. As a result, even for moderate values of the entangling power dual-unitary circuits produce 2-designs faster than Haar random circuits. Instead, away from the dual-unitary point the speed of 2-design preparation depends on both entangling power and dual-unitarity breaking. We argued that the production speed of more general k -designs should not only depend on the entangling power, however, we showed that dual-unitary circuits with maximal entangling power — perfect tensors [57–61] — give the optimal k -design preparation for any k . We also demonstrated numerically that, for $k = 3$, this is the case also for dual-unitary gates in the Hadamard family [51]. Our findings suggest that one can significantly improve the preparation of Haar random states by considering specific gates — dual-unitary with high entangling power — with a minimal amount of randomness. In a practical implementation this reduces both the required sample size and the time to run a single sample.

Moreover, we found that, in contrast to the random circuit setting, the k -design preparation in minimally random quantum circuits occurs in a two-step fashion — similarly to what happens for purity [30–32] and out-of-time-ordered correlators [33, 34] — and provided an analytic description of this phenomenon in the case of dual-unitary circuits. These findings suggest that that the two settings we studied here are more similar to each other than to Haar random circuits, meaning that the setting (b) represents a qualitatively more accurate modelling of non-random dynamics than the fully random circuit.

Our work raises many interesting questions for future research. In particular, we can identify two compelling directions. One is to rigorously prove some of the statements that are argued or conjectured here. For example, that the design production speed achieved by perfect tensors is the theoretical maximum achievable in a brickwork circuit and whether one can achieve this speed considering perfect tensors in the setting (a). The other is to ask, more generally, whether the our setting (a) is the optimal one for producing k -designs with a brickwork quantum circuit (i.e. the one requiring the least amount of resources) or can be further improved.

ACKNOWLEDGMENTS

We acknowledge financial support from the Royal Society through the University Research Fellowship No. 201101 (B. B. and J. R.) and the Leverhulme Trust through the Early Career Fellowship No. ECF-2022-324 (K. K.).

Appendix A: Proof of Property 1

Property 1 follows by straightforward adaptation of Ippoliti and Ho’s Theorem (cf. Sec. 3.C in Ref. [26]). Let us provide a brief proof considering separately the three Cases (a.1), (a.2), and (b.1).

1. Proof for Case (a.1)

In Case (a.1) the mixed state $\rho_t^{(k)}$ evolves according to

$$\rho_{t+1}^{(k)} = \mathcal{B}_k[\rho_t^{(k)}] = \mathcal{U}^{\otimes k} \mathcal{D}_k[\rho_t^{(k)}] (\mathcal{U}^\dagger)^{\otimes k} \quad (\text{A1})$$

where \mathcal{U} is written in terms of matrices $U^{(n)} \in \mathcal{A}_V$ as in Eq. (1) and

$$\mathcal{D}_k[\cdot] = 4^{-1} \sum_{\alpha \in \{I, \sigma^x, \sigma^y, \sigma^z\}} (\alpha_{2L})^{\otimes k} \cdot (\alpha_{2L})^{\otimes k}. \quad (\text{A2})$$

This is very similar to the setting considered in Ref. [26]: the only difference is that \mathcal{A}_V is an open subset of $U(4)$ and not necessarily of the dual-unitary submanifold. Therefore, we need to show that the Lemma in Appendix E of Ref. [26], the one guaranteeing that one can

approximate any unitary by a brickwork circuit of gates taken from \mathcal{A}_V , still holds. Repeating the arguments of Ref. [26] we then need to show that

$$(UW^\dagger)_{n,n+1}, \quad (\text{A3})$$

can generate any unitary operation by varying $n \in \mathbb{Z}_{2L}$, and $U, W \in \mathcal{A}_V$. Considering W close to U we see that one can then generate any arbitrary infinitesimal unitary transformation on the qubits at position n and $n+1$. Taking then sufficiently high powers one can generate any unitary transformation on the two qubits. Since n is arbitrary the statement immediately follows. Following Ref. [26] we then have that the limit

$$\rho_\infty^{(k)} = \lim_{t \rightarrow \infty} \rho_t^{(k)}, \quad (\text{A4})$$

exists and commutes with

$$(\mathcal{U} \sigma^\alpha \mathcal{U}^\dagger)^{\otimes k}, \quad (\text{A5})$$

where \mathcal{U} is an arbitrary unitary matrix in $U(2^{2L})$. These two matrices can be chosen in such a way to generate a complete gate set for each pair of qubits on the chain. Therefore, we conclude that $\rho_\infty^{(k)}$ commutes with any unitary matrix of the form $\mathcal{U}^{\otimes k}$, with \mathcal{U} in $U(2^{2L})$. The Schur–Weyl duality [64, 65] then implies that $\rho_\infty^{(k)} = \rho_H^{(k)}$.

2. Proof for Case (a.2)

In Case (a.2) the channel $\mathcal{B}_k[\cdot]$ can again be written as in Eq. (A1). In this case, however, d is a generic integer ≥ 2 and $\mathcal{D}_k[\cdot]$ is modified to

$$\mathcal{D}_k[\cdot] = \int_{U(d)} (\alpha)^{\otimes k} \cdot (\alpha_{2L}^\dagger)^{\otimes k} \mu_H(\alpha_{2L}), \quad (\text{A6})$$

Therefore the discussion in Ref. [26] does not directly apply. Specifically, we need to prove again the Lemmas in Appendix D of Ref. [26], those concerning the existence of the limit state and the fact that it commutes with the Krauss operators of the channel. By noting that, however, $\mathcal{D}_k[\cdot]$ projects the state at site $2L$ on the space spanned by $\{P_\sigma\}_{\sigma \in S_k}$, where S_k is the symmetric group of k elements and

$$[P_\sigma]_{i,j} = \prod_{p=1}^k \delta_{i_p, j_{\sigma(p)}}, \quad (\text{A7})$$

one finds that the arguments of Ref. [26] can be straightforwardly repeated and both Lemmas continue to hold. Also the Lemma in Appendix E holds as the arguments of the previous subsection are not restricted to $d = 2$. Therefore, we again have that the limit

$$\rho_\infty^{(k)} = \lim_{t \rightarrow \infty} \rho_t^{(k)}, \quad (\text{A8})$$

exists and commutes with

$$(\mathcal{U}u_{2L}\mathcal{U}^\dagger)^{\otimes k}, \quad (\text{A9})$$

where u is an arbitrary unitary matrix in $U(d)$ and \mathcal{U} is an arbitrary unitary matrix in $U(d^{2L})$. These two matrices can be chosen in such a way to generate a complete gate set for each pair of qudits on the chain. Therefore, we again conclude that $\rho_\infty^{(k)}$ commutes with any unitary matrix of the form $\mathcal{U}^{\otimes k}$, with \mathcal{U} in $U(d^{2L})$. The Schur–Weyl duality [64, 65] then implies that $\rho_\infty^{(k)} = \rho_H^{(k)}$.

3. Proof for Case (b.1)

The statement for Case (b.1) immediately follows from Case (a.2). One can first average only on the unitary at the boundary producing the channel studied in the previous subsection. Namely, the k -moment state is written as

$$\rho_t^{(k)} = \int \rho_t^{(k)}(\alpha) \prod_{j=1}^{2L-1} \prod_{\tau=1}^t \mu_H(\alpha_{2\tau-1}^{(j)}) \mu_H(\alpha_{2\tau}^{(j)}), \quad (\text{A10})$$

where the integrand is a step of evolution of the channel studied in the previous subsection for a given value of the one-site unitaries $\alpha = (\alpha_1^{(1)}, \dots, \alpha_{2t}^{(2L-1)})$. Therefore we readily have

$$\rho_\infty^{(k)} = \int \rho_H^{(k)} \prod_{j=1}^{4Lt-1} \mu_H(\alpha) = \rho_H^{(k)}. \quad (\text{A11})$$

Appendix B: Overlap-magnitude distribution

One can think of Eq. (10) as defining the moments of the overlap-magnitude distribution, i.e., the distribution of

$$|\langle \psi_z | \psi_q \rangle|, \quad (\text{B1})$$

and it is interesting to wonder what is the asymptotic form that this distribution takes in the large time limit. In this appendix we address this question.

First, let us derive an asymptotic form for the infinite-time expression in Eq. (12), where we take L to be large while keeping k fixed. In this case Stirling's approximation gives us

$$\left(F_H^{(k)}\right)^{-1} \sim \frac{\sqrt{1+\mu}}{k!} (1+\mu)^{d^{2L}-1} \left(\frac{d^{2L}+k-1}{e}\right)^k, \quad (\text{B2})$$

where we set $\mu = k/(d^{2L}-1)$. Therefore, at leading order we find

$$F_H^{(k)} \sim d^{-2kL} k!. \quad (\text{B3})$$

These moments coincide with those of the generalised gamma distribution [66]

$$p(x) = \frac{(p/a)^q x^{q-1}}{\Gamma(q/p)} e^{-(x/a)^p}, \quad (\text{B4})$$

for a specific choice of parameters a, p, q . In particular, recalling that the moments of the distribution in Eq. (B4) are given by

$$\mathbb{E}(X^r) = a^r \frac{\Gamma\left(\frac{q+r}{p}\right)}{\Gamma\left(\frac{q}{p}\right)}, \quad (\text{B5})$$

a direct comparison shows that the latter coincide with those in Eq. (B3) for $a = d^{-L}$, $q = p = 2$, and $r = 2k$.

For this specific choice of parameters, i.e. for $p = q = 2$, the distribution in Eq. (B4) is known as Rayleigh distribution [42] and arises, for instance, as the distribution of the magnitude of complex numbers that are generated by drawing their real and imaginary part independently from a Gaussian distribution with zero mean and unit variance.

Our numerical results suggest that the overlap magnitudes follow a Rayleigh distribution well beyond the asymptotic limits considered above and approach this universal form also for modest times and system sizes, see, e.g., Fig. 11.

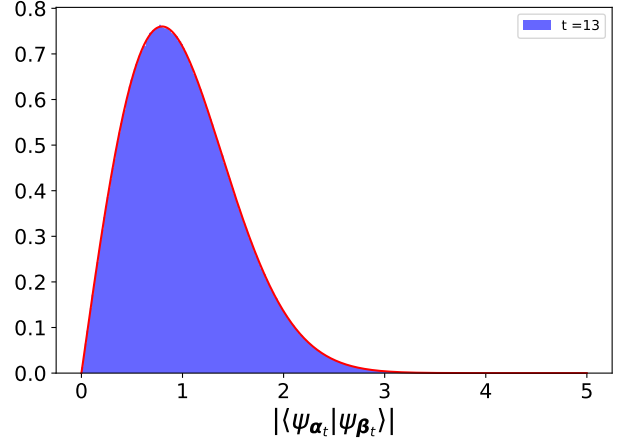


FIG. 11. Distribution of $|\langle \psi_{\alpha_t} | \psi_{\beta_t} \rangle|$ for $L = 6$, where we inserted Pauli random unitaries on the boundary and used 10^7 samples. In blue we showcase the actual sampled histogram while in red we showcase a fit to the generalised Gamma distribution, where we find $q = 1.9998$ and $p = 2.0009$. Data was generated for the DU point $\delta = 0$.

-
- [1] D. N. Page, Information in black hole radiation, *Phys. Rev. Lett.* **71**, 3743 (1993).
- [2] P. Hayden and J. Preskill, Black holes as mirrors: Quantum information in random subsystems, *J. High Energy Phys.* **2007** (09), 120.
- [3] H.-Y. Huang, R. Kueng, and J. Preskill, Predicting many properties of a quantum system from very few measurements, *Nat. Phys.* **16**, 1050 (2020).
- [4] J. Eisert, D. Hangleiter, N. Walk, I. Roth, D. Markham, R. Parekh, U. Chabaud, and E. Kashefi, Quantum certification and benchmarking, *Nat. Rev. Phys.* **2**, 382 (2020).
- [5] E. Knill, Approximation by quantum circuits, [arXiv:quant-ph/9508006](https://arxiv.org/abs/quant-ph/9508006) (1995).
- [6] J. Emerson, Y. S. Weinstein, M. Saraceno, S. Lloyd, and D. G. Cory, Pseudo-random unitary operators for quantum information processing, *Science* **302**, 2098 (2003).
- [7] A. Ambainis and J. Emerson, Quantum t -designs: t -wise independence in the quantum world, in *Twenty-Second Annual IEEE Conference on Computational Complexity (CCC'07)* (2007) pp. 129–140.
- [8] A. W. Harrow and R. A. Low, Random quantum circuits are approximate 2-designs, *Commun. Math. Phys.* **291**, 257 (2009).
- [9] F. G. S. L. Brandao and M. Horodecki, Exponential quantum speed-ups are generic, *Q. Inf. Comp.* **13**, 901 (2013).
- [10] F. G. S. L. Brandao, A. W. Harrow, and M. Horodecki, Local random quantum circuits are approximate polynomial-designs, *Commun. Math. Phys.* **346**, 397 (2016).
- [11] F. G. S. L. Brandão, A. W. Harrow, and M. Horodecki, Efficient quantum pseudorandomness, *Phys. Rev. Lett.* **116**, 170502 (2016).
- [12] N. Hunter-Jones, Unitary designs from statistical mechanics in random quantum circuits, [arXiv:1905.12053](https://arxiv.org/abs/1905.12053) (2019).
- [13] J. Haferkamp, Random quantum circuits are approximate unitary t -designs in depth $o(nt^{5+o(1)})$, *Quantum* **6**, 795 (2022).
- [14] J. Haferkamp, F. Montealegre-Mora, M. Heinrich, J. Eisert, D. Gross, and I. Roth, Efficient unitary designs with a system-size independent number of non-clifford gates, *Commun. Math. Phys.* **397**, 995 (2023).
- [15] S. N. Hearth, M. O. Flynn, A. Chandran, and C. R. Laumann, Unitary k -designs from random number-conserving quantum circuits, [arXiv:2306.01035](https://arxiv.org/abs/2306.01035) (2024).
- [16] T. Schuster, J. Haferkamp, and H.-Y. Huang, Random unitaries in extremely low depth, [arXiv:2407.07754](https://arxiv.org/abs/2407.07754) (2024).
- [17] C.-F. Chen, J. Haah, J. Haferkamp, Y. Liu, T. Metger, and X. Tan, Incompressibility and spectral gaps of random circuits, [arXiv:2406.07478](https://arxiv.org/abs/2406.07478) (2024).
- [18] N. LaRacuente and F. Leditzky, Approximate unitary k -designs from shallow, low-communication circuits, [arXiv:2407.07876](https://arxiv.org/abs/2407.07876) (2024).
- [19] H. Liu, A. Hulse, and I. Marvian, Unitary designs from random symmetric quantum circuits, [arXiv:2408.14463](https://arxiv.org/abs/2408.14463) (2024).
- [20] P. Calabrese, F. H. Essler, and G. Mussardo, Introduction to “Quantum integrability in out of equilibrium systems”, *J. Stat. Mech.: Theory Exp.* **2016** (6), 064001.
- [21] J. Eisert, M. Friesdorf, and C. Gogolin, Quantum many-body systems out of equilibrium, *Nat. Phys.* **11**, 124 (2015).
- [22] J. Choi, A. L. Shaw, I. S. Madjarov, X. Xie, R. Finkelstein, J. P. Covey, J. S. Cotler, D. K. Mark, H.-Y. Huang, A. Kale, *et al.*, Preparing random states and benchmarking with many-body quantum chaos, *Nature* **613**, 468 (2023).
- [23] J. S. Cotler, D. K. Mark, H.-Y. Huang, F. Hernández, J. Choi, A. L. Shaw, M. Endres, and S. Choi, Emergent quantum state designs from individual many-body wave functions, *PRX Quantum* **4**, 010311 (2023).
- [24] W. W. Ho and S. Choi, Exact emergent quantum state designs from quantum chaotic dynamics, *Phys. Rev. Lett.* **128**, 060601 (2022).
- [25] M. Ippoliti and W. W. Ho, Solvable model of deep thermalization with distinct design times, *Quantum* **6**, 886 (2022).
- [26] M. Ippoliti and W. W. Ho, Dynamical purification and the emergence of quantum state designs from the projected ensemble, *PRX Quantum* **4**, 030322 (2023).
- [27] R.-A. Chang, H. Shrotriya, W. W. Ho, and M. Ippoliti, Deep thermalization under charge-conserving quantum dynamics, [arXiv:2408.15325](https://arxiv.org/abs/2408.15325) (2024).
- [28] D. K. Mark, F. Surace, A. Elben, A. L. Shaw, J. Choi, G. Refael, M. Endres, and S. Choi, Maximum entropy principle in deep thermalization and in Hilbert-space ergodicity, *Phys. Rev. X* **14**, 041051 (2024).
- [29] B. Bertini, P. Kos, and T. Prosen, Exact correlation functions for dual-unitary lattice models in 1 + 1 dimensions, *Phys. Rev. Lett.* **123**, 210601 (2019).
- [30] J. Bensa and M. Žnidarič, Fastest local entanglement scrambler, multistage thermalization, and a non-hermitian phantom, *Phys. Rev. X* **11**, 031019 (2021).
- [31] M. Žnidarič, Solvable non-Hermitian skin effect in many-body unitary dynamics, *Phys. Rev. Res.* **4**, 033041 (2022).
- [32] M. Žnidarič, Phantom relaxation rate of the average purity evolution in random circuits due to Jordan non-Hermitian skin effect and magic sums, *Phys. Rev. Res.* **5**, 033145 (2023).
- [33] J. Bensa and M. Žnidarič, Two-step phantom relaxation of out-of-time-ordered correlations in random circuits, *Phys. Rev. Res.* **4**, 013228 (2022).
- [34] M. Žnidarič, Two-step relaxation in local many-body Floquet systems, *J. Phys. A: Math. Theor.* **56**, 434001 (2023).
- [35] R. Suzuki, H. Katsura, Y. Mitsuhashi, T. Soejima, J. Eisert, and N. Yoshioka, More global randomness from less random local gates, [arXiv:2410.24127](https://arxiv.org/abs/2410.24127) (2024).
- [36] C. Jonay and T. Zhou, Physical theory of two-stage thermalization, *Phys. Rev. B* **110**, L020306 (2024).
- [37] C. Jonay, C. Li, and T. Zhou, Two-stage relaxation of operators through domain wall and magnon dynamics, [arXiv:2411.07298](https://arxiv.org/abs/2411.07298) (2024).
- [38] With obvious modifications this also applies for continuous probability measures.
- [39] P. W. Claeys and A. Lamacraft, Emergent quantum state designs and biunitarity in dual-unitary circuit dynamics, *Quantum* **6**, 738 (2022).
- [40] J. M. Renes, R. Blume-Kohout, A. J. Scott, and C. M.

- Caves, Symmetric informationally complete quantum measurements, *J. Math. Phys.* **45**, 2171 (2004).
- [41] D. A. Roberts and B. Yoshida, Chaos and complexity by design, *J. High. Energy Phys.* **2017**, 1 (2017).
- [42] A. Papoulis and S. Pillai, *Probability, Random Variables, and Stochastic Processes*, McGraw-Hill series in electrical engineering: Communications and signal processing (Tata McGraw-Hill, 2002).
- [43] I. Bengtsson and K. Życzkowski, *Geometry of Quantum States: An Introduction to Quantum Entanglement* (Cambridge University Press, 2007).
- [44] We use $|\lambda_m|$ without an additional subscript whenever we want to refer to the magnitude of the eigenvalue.
- [45] B. Bertini, P. Kos, and T. Prosen, Entanglement spreading in a minimal model of maximal many-body quantum chaos, *Phys. Rev. X* **9**, 021033 (2019).
- [46] L. Piroli, B. Bertini, J. I. Cirac, and T. Prosen, Exact dynamics in dual-unitary quantum circuits, *Phys. Rev. B* **101**, 094304 (2020).
- [47] G. Köstenberger, Weingarten calculus, [arXiv:2101.00921](https://arxiv.org/abs/2101.00921) (2021).
- [48] R. Suzuki, K. Mitarai, and K. Fujii, Computational power of one- and two-dimensional dual-unitary quantum circuits, *Quantum* **6**, 631 (2022).
- [49] A. Foligno and B. Bertini, Growth of entanglement of generic states under dual-unitary dynamics, *Phys. Rev. B* **107**, 174311 (2023).
- [50] P. Zanardi, C. Zalka, and L. Faoro, Entangling power of quantum evolutions, *Phys. Rev. A* **62**, 030301(R) (2000).
- [51] S. Aravinda, S. A. Rather, and A. Lakshminarayan, From dual-unitary to quantum Bernoulli circuits: Role of the entangling power in constructing a quantum ergodic hierarchy, *Phys. Rev. Research* **3**, 043034 (2021).
- [52] S. A. Rather, S. Aravinda, and A. Lakshminarayan, Creating ensembles of dual unitary and maximally entangling quantum evolutions, *Phys. Rev. Lett.* **125**, 070501 (2020).
- [53] S. A. Rather, S. Aravinda, and A. Lakshminarayan, Construction and local equivalence of dual-unitary operators: From dynamical maps to quantum combinatorial designs, *PRX Quantum* **3**, 040331 (2022).
- [54] B. Bertini and L. Piroli, Scrambling in random unitary circuits: Exact results, *Phys. Rev. B* **102**, 064305 (2020).
- [55] C. Jonay, D. A. Huse, and A. Nahum, Coarse-grained dynamics of operator and state entanglement (2018), [arXiv:1803.00089](https://arxiv.org/abs/1803.00089) [cond-mat.stat-mech].
- [56] T. Zhou and A. Nahum, Entanglement membrane in chaotic many-body systems, *Phys. Rev. X* **10**, 031066 (2020).
- [57] F. Pastawski, B. Yoshida, D. Harlow, and J. Preskill, Holographic quantum error-correcting codes: Toy models for the bulk/boundary correspondence, *J. High Energy Phys.* **2015** (6), 1.
- [58] W. Helwig, W. Cui, J. I. Latorre, A. Riera, and H.-K. Lo, Absolute maximal entanglement and quantum secret sharing, *Phys. Rev. A* **86**, 052335 (2012).
- [59] W. Helwig, Absolutely maximally entangled qudit graph states (2013), [arXiv:1306.2879](https://arxiv.org/abs/1306.2879) [quant-ph].
- [60] P. Facchi, G. Florio, G. Parisi, and S. Pascazio, Maximally multipartite entangled states, *Phys. Rev. A* **77**, 060304 (2008).
- [61] D. Goyeneche, D. Alsina, J. I. Latorre, A. Riera, and K. Życzkowski, Absolutely maximally entangled states, combinatorial designs, and multiunitary matrices, *Phys. Rev. A* **92**, 032316 (2015).
- [62] F. Huber, C. Eltschka, J. Siewert, and O. Gühne, Bounds on absolutely maximally entangled states from shadow inequalities, and the quantum MacWilliams identity, *J. Phys. A: Math. Theor.* **51**, 175301 (2018).
- [63] S. A. Rather, A. Burchardt, W. Bruzda, G. Rajchel-Mieldzióć, A. Lakshminarayan, and K. Życzkowski, Thirty-six entangled officers of Euler: Quantum solution to a classically impossible problem, *Phys. Rev. Lett.* **128**, 080507 (2022).
- [64] W. Fulton and J. Harris, *Representation Theory: A First Course*, Graduate Texts in Mathematics (Springer New York, 1991).
- [65] I. Marvian and R. W. Spekkens, A generalization of Schur–Weyl duality with applications in quantum estimation, *Commun. Math. Phys.* **331**, 431 (2014).
- [66] E. W. Stacy, A generalization of the gamma distribution, *Ann. Math. Statist.* **33**, 1187 (1962).